MULTI-GIGABIT TRANSMISSION OVER MULTIMODE OPTICAL FIBRE

THEORY AND DESIGN METHODS FOR 10GbE SYSTEMS

Stefano Bottacchi

Formerly with Infineon Technology AG,
Fiber Optic, Concept Engineering, Germany

John Wiley & Sons, Ltd

MULTI-GIGABIT TRANSMISSION OVER MULTIMODE OPTICAL FIBRE

MULTI-GIGABIT TRANSMISSION OVER MULTIMODE OPTICAL FIBRE

THEORY AND DESIGN METHODS FOR 10GbE SYSTEMS

Stefano Bottacchi

Formerly with Infineon Technology AG,
Fiber Optic, Concept Engineering, Germany

John Wiley & Sons, Ltd

John Wiley & Sons Ltd, The Atrium, Southern Gate, Chichester,
West Sussex PO19 8SQ, England

Telephone (+44) 1243 779777

Email (for orders and customer service enquiries): cs-books@wiley.co.uk
Visit our Home Page on www.wiley.com

Other Wiley Editorial Offices

John Wiley & Sons Inc., 111 River Street, Hoboken, NJ 07030, USA

Jossey-Bass, 989 Market Street, San Francisco, CA 94103-1741, USA

Wiley-VCH Verlag GmbH, Boschstr. 12, D-69469 Weinheim, Germany

John Wiley & Sons Australia Ltd, 42 McDougall Street, Milton, Queensland 4064, Australia

John Wiley & Sons (Asia) Pte Ltd, 2 Clementi Loop #02-01, Jin Xing Distripark, Singapore 129809

John Wiley & Sons Canada Ltd, 6045 Freemont Blvd, Mississauga, ONT, L5R 4J3, Canada

Wiley also publishes its books in a variety of electronic formats. Some content that appears in print may not be available in electronic books.

Library of Congress Cataloging-in-Publication Data:

Bottacchi, Stefano.
Multi-gigabit transmission over multimode optical fibre : theory and design methods for 10GbE systems / Stefano Bottacchi.
p. cm.
Includes bibliographical references and index.
ISBN-13: 978-0-471-89175-8 (cloth : alk. paper)
ISBN-10: 0-471-89175-4 (cloth : alk. paper)
1. Optical communications. 2. Fiber optics. I. Title.
TK5103.59.B68 2006
621.382′7 – dc22

2006014654

British Library Cataloguing in Publication Data

A catalogue record for this book is available from the British Library

ISBN-13: 978-0-471-89175-8
ISBN-10: 0-471-89175-4

Typeset in 9/11pt Times by Laserwords Private Limited, Chennai, India
Printed and bound in Great Britain by Antony Rowe Ltd, Chippenham, Wiltshire
This book is printed on acid-free paper responsibly manufactured from sustainable forestry in which at least two trees are planted for each one used for paper production.

To my wife Laura
and my daughters
Francesca and Alessandra

Contents

Preface

Fast-growing Ethernet demands in the metropolitan area networking have very recently caused the IEEE 802.3 Standardization Committee to develop new transmission system specifications for end-user 10GbE applications over existing multimode optical fiber with a target reach of at least three hundred meters. However, high-speed transmission at multigigabit data rates, combined with the existing multimode optical fiber infrastructure, have led to relevant optical pulse distortion even after only one hundred meters of link length, consequently demanding proper compensation techniques of the time dispersion.

In order to understand better how simultaneous multipath optical pulse dispersion, intersymbol interference (ISI) and several noise sources affect the multigigabit transmission performances over multimode fibers, a detailed analysis of the optical propagation mechanisms has been developed thoroughly in this book. The general theoretical approach favors mathematical modeling, which is better suited to the modular structure of every analytical link simulator. After introducing the physical concepts and the mathematical modeling, each chapter reports extensive working examples based on the developing software Matlab® 7.1 from The MathWorks, Inc. However, despite using an original theoretical approach, this book would not have been complete without the extensive experimental verification reported in the last part of this work, which refers to the pioneering transmission experiments of 10GbE over legacy multimode fibers recently performed at the Fiber Optic Laboratory of Infineon Technologies AG, Berlin.

Multigigabit transmission over multimode optical fiber could never be achieved without implementing proper pulse dispersion equalization techniques. The electronic dispersion compensator (EDC) emerges today as the key factor in achieving the required performance in practical implementations and has accordingly a very relevant role to play in the book. The theoretical approach followed identifies first the ideal inverse linear filtering as the reference compensation method for every pulse dispersion mechanism, in order to qualify and compare more sophisticated equalizing solutions. Although it is well known that inverse linear filtering does not represent a suitable solution, especially under severe signal degradation, its simple and ideal compensation principle makes this filter well suited as the reference dispersion compensator.

The most promising electronic dispersion compensator (EDC) available at the 10GbE data rate and suitable for mass volume access networking is based on the dispersion feedback equalizer (DFE). The theory and the modeling of the dispersion feedback equalizer are presented, based on the minimum mean square error criteria as originally proposed by J. Salz at the beginning of the 1970s. Several numerical calculations of the optical channel metrics follow. It is outside the scope of this book to present equalization techniques based on different approaches like the maximum likelihood sequence equalizer (MLSE). However, the main effort has been spent in identifying ideal system performances, design criteria and limitations inherent to different pulse dispersion mechanisms occurring in multimode optical fibers in order to achieve the required transmission performances.

Stefano Bottacchi
Milan

Book Organization

The book is divided into two parts. The first part deals with the theory and the modeling of the multimode optical fiber propagation, leading to useful closed-form equations well suited for analytical simulation purposes. Particular attention has been devoted to the theoretical modeling of the multimode fiber impulse response, including both the chromatic and the modal responses. A mathematical modeling approach has been preferred in order to arrive at a set of equations suitable for a multimode optical fiber transmission link simulator. The Gaussian response model has been detailed with several numerical examples. The second part deals instead with the optoelectronic subsystems encountered in the implementation of the multigigabit transmission system using the multimode optical fiber. The optical transmitter, the optical receiver and, in particular, the electronic dispersion compensator have been exhaustively analyzed and specified in order to give to the reader the essential directions for proceeding further in the system design optimization. Several experimental results have been added at the end of the book in order to emphasize the open issues and the distance still encompassing the performances required for massive deployment and the state-of-the-art experimental laboratory implementation of 10GbE transmission over multimode optical fibers.

Looking into a more detailed organization of the book, the first chapter serves as the general introduction to the field and overviews almost all aspects developed in subsequent chapters. In particular, Chapter 1 introduces the basic transmission methods and issues encountered when sending multigigabit data over multimode optical fibers. Chapter 2 presents an original analysis of a metallic-based transmission waveguide, leading to different response behaviors used for comparison purposes with the simple Gaussian response model of multimode optical fibers. Chapter 3 to Chapter 7 deal with the propagation theory and modeling of the multimode fibers. Chapter 3 reviews the multimode fiber theory by introducing the principal concepts, parameters and mathematical tools needed for the subsequent development. Chapter 4 presents the theory of the chromatic dispersion in multimode fibers assuming a general multimode source spectrum profile and an arbitrary group delay distribution. The developed theory leads to a closed-form mathematical expression for the chromatic impulse response. Chapter 5 approaches the theory of the modal dispersion assuming a general group delay distribution and modal excitation. The general expression derived for the impulse response includes both embedded effects of chromatic and modal dispersions. Several Matlab® codes written ad hoc provide interesting and original simulation cases for underlying basic physical principles and interaction mechanisms occurring with the total pulse dispersion. Chapter 6 reports the Gaussian model of the multimode fiber response, including benefits and limitations of this easy mathematical approach. Several useful formulas and numerical examples close the chapter. Chapter 7 introduces some important topics encountered in high-speed transmission using multimode fiber. Computer modeling provides interesting examples of impulse response compositions including pulse precursors and postcursors. The modal theory of the step-index fiber is presented as the simpler case for introducing launching condition issues in more complex graded refractive index fibers.

The second part of the book starts with Chapter 8, which introduces the characteristics and gives modeling suggestions for the principal transmission system components. Several optical waveforms are considered and compared as potential light sources for multigigabit transmission. The general architecture of the optical receiver is then analyzed, including the characterization of topic receiving filter models, and a short theoretical approach is given to the intersymbol interference pattern. Chapter 9 presents the theoretical background for the equalization problem in multimode fiber transmission systems. The chapter starts by introducing the noise analysis and the error probability formulation in optical receivers. The ideal inverse filter is then proposed as the reference linear equalizer and the related noise enhancement factor is defined in order to make a quantitative comparison among different solutions. The eye diagram closure and more generally the optical power penalty are among the most relevant engineering tools used for assigning quantitative figures of merit to different equalizer structures. Chapter 10 presents the theory of the decision feedback equalizer as the basic building block of the electronic dispersion compensator solution today, and is proposed as the best solution for achieving 10GbE access networking over the legacy multimode fiber infrastructure. The concept of the channel metric as the measure of the optical power penalty formed by the linear transmission channel is then introduced. Quantitative measures of the linear channel performance, like PIE-L and PIE-D, are defined and compared with the power penalty due to noise enhancement of the ideal inverse linear equalizer. The last Chapter 11 is completely devoted to reporting the transmission experiments performed at the Fiber Optic Laboratory, Infineon Technology AG, Berlin, during 2003–2005. Details of the pulse responses of benchmark multimode fiber and the eye diagram measured at the 10GbE data rate are presented and correlated with system performances. New observations regarding the polarization-induced pulse distortion in multimode fiber links excited with offset launching are then presented. A first theoretical justification of the observed alterations is also approached. The last section reports the first EDC-based multigigabit transmission experiments carried out over multimode fibers. Transmission system performances including sample EDCs are finally evaluated by means of measured bit error rates.

Acknowledgments

The author is personally responsible for all the contents of this book, but feels personally indebted for the beautiful environment and the intellectual creative atmosphere he found at the former Concept Engineering Department of Fiber Optic, Infineon Technologies AG, Berlin, where most of the book content has been conceived. In particular, he is pleased to thank personally former colleagues Mr Jens Fiedler and Dr Joerg Kropp for providing stimulating discussions and leading experiments that guided almost all of the transmission measurements presented in this book.

Finally, yet importantly, the author is grateful to his family and parents who helped during the long development of the book with unlimited trust and patience.

Stefano Bottacchi
Milan

1

Introductory Concepts

Components and Design Issues for a Multigigabit Link over Multimode Fiber

1.1 Introduction

The recent huge demand for Multigigabit Ethernet (10GbE) and Fiber Channel (FC) standard applications in metropolitan areas has very rapidly pushed up the need for broader modulation frequency ranges in deployed multimode optical fibers. Since the beginning of the Gigabit Ethernet (GbE) in 1997, a great effort has been devoted to qualify transmission performances of standard multimode fiber (MMF) deployed in buildings, offices and everywhere around metropolitan areas. Multimode fibers had been developed in the past 20 years and an increase in optical fiber manufacturing and very different manufacturing procedures led to a very different transmission behavior and modal bandwidth optimization. At the beginning of the optical fiber transmission era, about 30 years ago, multimode fibers were deployed for use with light emitting diodes (LED) and low-bit-rate-based optical links, usually operating below 200 Mb/s. Since the advent of the Gigabit Ethernet during the late 1990s, the expected bit rate today has increased demand for multigigabit Internet routing in the metropolitan area, but this may not be possible due to the inherently slow transmission properties of the deployed multimode optical fibers. The transmission speed is no more than 1 Gb/s but 10 Gb/s and beyond are today requested for MMF links from most of the service providers.

Most of the installed multimode fiber base was manufactured during the 1980s and early 1990s, when the multimode optics was conceived essentially for subgigabit transmission applications, using surface emitting LED and large area PIN diodes operating mainly at 850 nm. High-speed optical transmission was concentrated on single-mode fiber technology where high transmission capacity easily allowed 10 Gb/s transmission over several tens of kilometers. High-speed telecommunication was concentrated mainly in the backbone market, where huge transmission capacities were needed to link large and faraway metropolitan areas. As soon as the Internet started to grow more quickly in the local area network, there was a need to increase the transmission capacity of the existing fiber infrastructure. That layout was structured with multimode fiber of use only for previous low-speed applications and the need for new engineering challenges in utilizing deployed multimode fibers at 10 Gb/s appeared as one of the major tasks facing the datacommunication industry. Efficient light sources such as the vertical cavity surface emitting laser (VCSEL) are suitable candidates for high-speed direct modulation, but they require new investigations on the effect of launching conditions

Multi-Gigabit Transmission over Multimode Optical Fibre: Theory and Design Methods for 10GbE Systems Stefano Bottacchi

on multimode fiber propagation behavior. The conventional multimode fiber coupling technology must be revised to take account of the new laser launching and multigigabit data rate, including fusion splices, connectors and optical couplers. Because of the complexity and the relevance of these applications, the new standard 10BASE-LRM is under development by the IEEE802.3ae committee.

1.2 Multimode Optical Fibers

Optical fibers have been widely deployed to serve extremely high performing transmission channels for both telecommunication and datacommunication applications since their first industrial manufacture in the mid seventies. For almost thirty years, optical fibers have represented the best transmission channel technology available for either long-reach backbone transmission or large local area distribution purposes. In order to serve a multigigabit transmission medium every wired transmission channel should have simultaneously low attenuation and high bandwidth per unit length. Optical fiber meets both of these requirements. Optical attenuation in fact ranges between 0.2 and 2.0 dB/km while the modulation bandwidth is inherently almost infinite in single-mode fibers for most telecommunication applications. In general, it is not possible to specify just one number to characterize either the attenuation or the modulation bandwidth of optical fiber because both parameters are strongly influenced by the operating wavelength and optical waveguide structure. For example, in the limiting case of single-mode optical fiber linearly excited by a highly coherent externally modulated laser source the link bandwidth is limited only by the modulating signal bandwidth and by fiber polarization mode dispersion. Under these conditions, ITU-T STM16 transmission at 2488 and 320 Mb/s can reach more than 1000 km at 1550 nm without being particularly limited by pulse dispersion of the bandwidth limitation. However, even the extremely low attenuation of less then 0.2 dB/km available at 1550 nm would require a link budget of 200 dB in order to be connected. This extremely high attenuation can be overcome by using optical amplifiers with a repetition span of about 25 dB between each of them.

The picture is completely different when using multimode optical fibers. Before entering into more detail, it is useful first to describe the waveguide properties of optical fibers. The optical fiber is a cylindrical dielectric waveguide where the guiding principle is achieved using the refractive index difference between the inner dielectric region, the core and the outside dielectric region, the cladding. Making the refractive index slightly higher in the core than in the cladding ensures optical waveguide operation in a specific wavelength range.

The optical fiber dealt with here is made of a silica glass composition and both the core and the cladding must be carefully doped and processed in order to obtain the exact refractive index profile and high-purity material needed to achieve simultaneously very low dispersion and attenuation. The low attenuation wavelength range is achieved by choosing the correct silica glass to place the dielectric optical waveguide structure within the near-infrared region, $820\,\text{nm} < \lambda < 1620\,\text{nm}$. In this wavelength range, the optical fiber will perform in the single-mode or multimode regimes depending on the radius a of the inner core region. Standard single-mode fibers have the core diameter close to $a = 4\,\mu\text{m}$ or less, while standard multimode fibers have a much larger core radius, either $a = 25\,\mu\text{m}$ or $a = 31.25\,\mu\text{m}$. Other factors affect the modal capability of the fiber, but essentially the core diameter is mainly responsible for the different kinds of waveguide behavior. Figure 1.1 shows a schematic drawing of the multimode fiber geometry.

This book will deal exclusively with multimode fibers, so cylindrical dielectric waveguides made of doped silica glass with a core diameter of either $50\,\mu\text{m}$ or $62.5\,\mu\text{m}$ will be referred to implicitly. These multimode fibers are specified by ISO/IEC 11801 and ITU-T G.651 standards. The multimode regime requires a strong bandwidth limitation compared to single-mode ones. This is essentially because of the multipath propagation and the related group delay per unit length spreading among

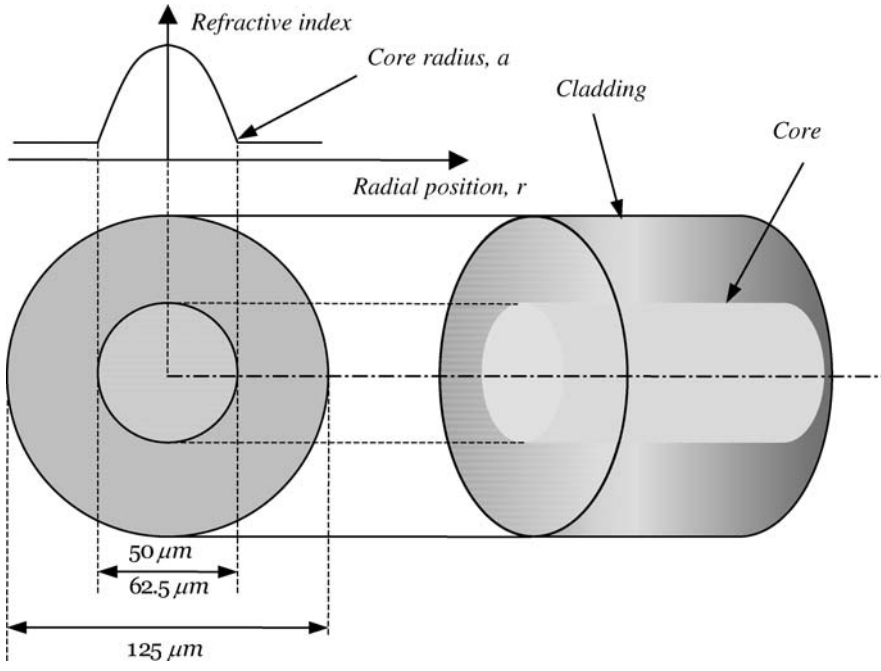

Figure 1.1 Multimode fiber geometry

all allowed and excited modes. The refractive index profile is the only functional parameter that sets the electromagnetic properties of every dielectric waveguide. In order to compensate for different mode delays it is possible to design a graded refractive index profile. Accordingly, the mode delay per unit length is equalized and in principle the modal bandwidth would be infinitely large for perfectly compensated delays. In reality, group delay compensation is an extremely critical function of the refractive index profile and even assuming a highly sophisticate manufacturing process the highest modal bandwidth achieved for commercially available optical fiber usually does not exceed a few gigahertz per kilometer. In addition to modal dispersion, each mode is subjected to intrinsic chromatic dispersion due to the dispersion relationship between the modal propagation constant and the source spectrum width. Chromatic dispersion is otherwise identified as group velocity dispersion (GVD) and is the major drawback in dispersion-limited transmission using single-mode fiber with direct modulated semiconductor laser diode sources.

Every nonlinear behavior and dispersion contribution to pulse propagation experienced by single-mode fiber transmission would in principle be present even for each individual mode of every multimode fiber. Of course, the very different timescales of these phenomena with respect to modal dispersion makes the contribution of almost all of them negligible when considering pulse dispersion in multimode fibers. Accordingly, in the following chapters the theory of the multimode pulse response will be presented, including only modal and chromatic dispersion.

1.3 Semiconductor Laser Sources

There is a need to increase the transmission bit rate for high-speed laser sources, due to well-performing and low-cost direct modulation capabilities of those devices compared with the slow

and much less efficient LED. Recently, VCSEL technology provides a very interesting compromise in terms of speed, cost, yields and power consumption. However, more consolidated light sources for 10GbE, at least in the 1310 nm wavelength range, are still directly modulated Fabry-Perot (FP) lasers and distributed feedback (DFB) lasers. Unfortunately, any kind of laser source is almost a nightmare for every multimode fiber.

There are at least three characteristics of semiconductor lasers that act against the natural behavior of any multimode optical waveguide and of the multimode fiber in particular:

1. The light emitted from the semiconductor laser is spatially localized on to a region that is usually much narrower then the fiber core area. This leads to a partial excitation of a few mode groups allowed by the fiber. If the group delay of the multimode fiber is not compensated enough among excited bound modes (the amount of compensation required depends on the ratio between the bit rate and the differential mode delay), the energy distribution among a few excited modes will result in a consistent pulse broadening at the fiber end facet after just a few hundred meters of propagation length.
2. The laser coherence properties in conjunction with multimode connectors originate in the intensity-dependent Speckle noise term, namely the modal noise.
3. The power distribution among fiber modes is strongly dependent on the combined effect of launch polarization and environmental induced stresses and perturbation, originating in random output pulse fluctuations, which of course make the channel picture even more complicated.

A large number of measurements demonstrates how unpredictable the MMF frequency response would be when the light excitation comes from a laser source. The reason for such unpredictable behavior results from the very spatially localized excitation of a subset of guided modes in the MMF. Depending on which fiber modes are excited by the laser light, either a very high or a very low propagation bandwidth can be experienced on the same MMF link. When the light power is distributed among a few supporting modes, even a small propagation delay difference among excited modes will make a strong output pulse deformation with the creation of relatively large pulse precursors and postcursors that destroy pulse symmetry.

The launching-dependent frequency response of every multimode optical fiber clearly complicates the picture of multigigabit transmission over this dielectric waveguide. The IEEE802.3ae standard for 1GbE specifies the restricted offset launch conditions as the solution to provide suitable fiber mode excitation in order to control differential mode delay and pulse broadening. Even if restricted offset launch conditions provide a more stable multimode fiber bandwidth behavior, their implementation is not so simple as to be widely accepted and leads to increasing cost per module and other practical implications.

1.4 Offset Launch Conditions

A standard solution proposed to improve the multimode fiber bandwidth by limiting multipath propagation relies on specified offset launch conditions and related encircled flux specifications using standard offset launching patchcord. The idea behind offset launching is to excite selectively high-order modes that are localized in the mid-region of the fiber core section. Figure 1.2 shows qualitatively the offset launch case.

Unfortunately, offset launch patchcord is almost impractical today because of its dimensions and the space required to be hosted into small modules or crowded boards, as well as the cost issue. Sometimes, the cost of offset launching patchcord is comparable to the cost of the whole module. In addition, a unique solution for defining offset launch compliant with both 50 μm and 62.5 μm multimode fibers is still under study.

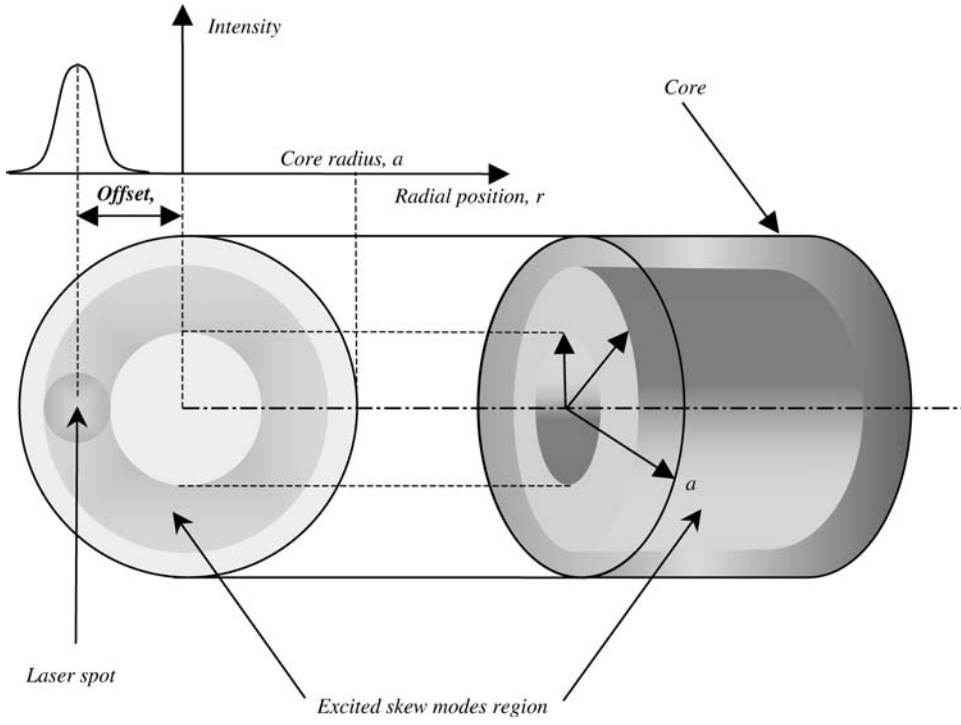

Figure 1.2 Schematic representation of the offset launch in a multimode fiber. The offset coordinate is ρ. Excited skew modes occupy the inner shaded region around the radial position ρ, leaving both the central region and the outer core region almost unoccupied by the electromagnetic energy

1.5 Optical Receivers

The optical receiver converts the optical signal available at the fiber end section into the corresponding electrical signal. This process takes place inside the optical photodetector according to the photoelectric effect. Each incoming photon has a probability of being absorbed, releasing its energy to a conduction band electron. The probability of photodetection depends on several factors involving the detector optical coupling, antireflection coating, depth of the intrinsic absorbing region, leakage currents and so on. All of these factors are usually summarized using a single parameter, namely the photodetector external quantum efficiency, $\eta_p(\lambda)$. Typical values range between $50\,\% < \eta_p(\lambda) < 95\,\%$, depending on the operating wavelength and photodetector structure. Very high-speed photodiodes have among the lowest quantum efficiency values due to width shortening of the absorbing region, thus minimizing the transit time dispersion. Coaxial receptacle photodiodes, designed for 10GbE applications in the second window operations $\lambda = 1310\,\text{nm}$, usually have quantum efficiency in the order of $60\,\% < \eta_p(\lambda) < 80\,\%$.

Each photon brings a fixed energy amount depending on its wavelength. The detected photon rate, namely the number of photons per unit time incident on the photodetector sensible area, is therefore related to the received optical power. The conversion factor is the universal constant R_0:

$$R_0 = \frac{q\lambda}{hc} \quad \text{(A/W)} \tag{1.1}$$

Substituting the speed of light in a vacuum, $c = 2.9979 \times 10^8$ m/s, and the electron charge, $q = 1.6022 \times 10^{-19}$ C, for the Plank constant, $h = 6.626110^{-34}$ J s, the following value for the conversion factor as a function of the wavelength is obtained:

$$R_0 = 0.8066\lambda_{[\mu m]} \Rightarrow \begin{cases} \lambda = 0.850\,\mu m \rightarrow R_0 = 0.686\,A/W \\ \lambda = 1.310\,\mu m \rightarrow R_0 = 1.057\,A/W \\ \lambda = 1.550\,\mu m \rightarrow R_0 = 1.250\,A/W \end{cases} \tag{1.2}$$

The product of the conversion factor $R_0(\lambda)$ with the photodetection external quantum efficiency $\eta_p(\lambda)$ defines the photodetector responsivity $R(\lambda)$:

$$R(\lambda) = R_0(\lambda)\eta_p(\lambda) = \frac{q\lambda}{hc}\eta_p(\lambda) \quad (A/W) \tag{1.3}$$

Assuming that the photodetection external quantum efficiency $\eta_p(\lambda) = 0.7$ is independent of the operating wavelength, from Equation (1.2) the following expected values of photodiode responsivity for 10GbE applications are obtained:

$$\eta_p = 0.7 \Rightarrow \begin{cases} \lambda = 0.850\,\mu m \rightarrow R_0 = 0.480\,A/W \\ \lambda = 1.310\,\mu m \rightarrow R_0 = 0.740\,A/W \\ \lambda = 1.550\,\mu m \rightarrow R_0 = 0.875\,A/W \end{cases} \tag{1.4}$$

It should be noted, however, that the photodetection external quantum efficiency is a decreasing function of the wavelength. This effect compensates partly for the linear reduction of the conversion constant in Equation (1.2) at shorter wavelengths.

The photocurrent is proportional to the envelope of the received optical intensity, and for this behavior the photodiode is defined as a square-law device. The optical power is then converted into electrical current intensity, as clearly reported by the unit of measure of the responsivity function in Equation (1.3). At a limited input optical power level, the photodiode behaves linearly with respect to the incident optical intensity and can be conveniently characterized by the impulse response and the transfer function in the frequency domain. The photodetector therefore performs the first filtering process on the incoming optical signal. The photocurrent pulses are then amplified and converted into more suitable voltage pulses before being processed through conventional clock and data recovery (CDR) circuits. If the multimode fiber bandwidth together with additional electrical low-pass filtering in the optical receiver front end set severe limitations on the signal available at the receiver decision section, a large error rate would be expected and a transmission failure status would therefore be detected. This failure mechanism is referred to as the 'dispersion limited system fault'. The only possible remedies known to overcome this fault condition is either to provide a received pulse reshaping process or to use error correcting code transmission or even reduce the signal bandwidth requirement in the given transmission channel using a proper modulation format. The first approach leads to the electronic dispersion compensation (EDC) technique, while two other solutions, optical mode filtering (OMF) and the multilevel modulation format (PAM-4), tend to either increase the multimode fiber transmission capacity or reduce the signal bandwidth occupation.

1.6 Signal Compensation Techniques

Due to the relatively large differential mode delay (DMD) encountered in multimode fibers when excited by semiconductor laser sources, a strong pulse dispersion and interferometric noise (Speckle pattern) are simultaneously expected as major limitations to multigigabit data transmission over a few hundred meters of link length. These effects lead to different dispersion compensation approaches, namely electronic dispersion compensation (EDC), optical mode filtering (OMF) and

quaternary pulse amplitude modulation (PAM-4). The IEEE 802.3aq 10BASE-LRM Committee is at present carefully investigating these three alternative compensating procedures.

The impulse response of a multimode fiber link distributed over several connected sections is very sensitive to perturbing environmental conditions like temperature mechanical vibration and even the state of polarization. Due to its inherent adaptive architecture, EDC seems to have better control against those environmental effects, making the multimode fiber link more robust under cabled operating conditions. However, it is widely accepted by the IEEE 802.3aq Committee that the complete picture of 10GbE over long-reach multimode fibers remains quite troublesome unless a proper dispersion compensation mechanism is taken into account. Although EDC seems to be the most promising solution for multipath pulse dispersion compensation, the remaining two approaches are still under investigation and merit some attention as alternative methods for potential future approaches. In the following, the operating principles of the above-mentioned three methods will be considered. All of the considered solutions have several issues to be solved in order to become widely deployed on the 10GbE large-volume market expected in 2006 and 2007. The basic principles of these signal compensation techniques for multigigabit transmission over multimode optical fibers will also be reviewed.

1.6.1 Electronic Dispersion Compensation (EDC)

The electronic dispersion compensation (EDC) technique proposes to mitigate optical pulse broadening at the multimode fiber output by means of electronic signal processing directly operating at the signal rate. The optical signal must be first detected and linearly amplified by a proper low-noise receiver before being processed by EDC. This approach requires relatively complex digital signal processing at 10 Gb/s in the case of the 10BASE-LRM standard. The key element is the adaptive finite impulse response (FIR) filter whose tap coefficients are managed through the minimum mean square error (MMSE) algorithm. Among several different available architectures the most suitable for achieving simultaneously a high bit rate capability and relatively low power requirements is based on a combination of the *feedforward equalizer* (FFE) and the *decision feedback equalizer* (DFE). Both sections are realized by means of FIR filters. Key parameters of both the FFE and DFE are the number of taps and the tap delay (tap spacing) used to synthesize each FIR filter. The more dispersed equalizer is expected to be the input pulse and the longer are would be the filter length in order to compensate for longer precursors and postcursors. This produces a trade-off between technological complexity, power consumption and compensation capability. Essentially, the EDC action can be depicted in two steps:

1. The FFE section controls the input pulse shape providing weighted amounts of frequency response equalization in order to re-establish a proper pulse profile, thus reducing the intersymbol interference pattern.
2. The DFE section adaptively adjusts the decision threshold of the digital quantizer in order to minimize the intersymbol interference power at the decision section output. According to standard solutions, the DFE operation requires the clock recovery feature from the incoming data pattern in order to synchronize the decision timing properly.

In this context, relatively relaxed optical constraints including launch conditions, connector tolerances and optical detection architectures are required for the fiber transmission system. The EDC advantage relies on its integrated circuit (IC) structure: low cost, high reliability, compact and easily integrable in a small form factor and pluggable data communication modules. The EDC drawback is that some unstable convergence is experienced when the required filter length increases and the multimode fiber response demands that the compensation capabilities be limited. A low value of the signal-to-noise ratio (SNR) at the optical receiver input places one more constraint on EDC

operation. The electronic compensator architecture should also include an adaptive electrical filter in order to track the compensation profile variations according to the temporal changes of the MMF response and to restore the proper electrical pulse profile at the decision section.

It will be seen in the next chapters that several fiber modes excited by the laser source will propagate, with relative delay differences giving rise to multipath pulse distortion after some distance from the launch section. Due to the large-area photodetection mechanism, interferometric noise plays a marginal role, leaving the complete interferometric pattern inside the detected light area. Spatial averaging over the whole fiber end section due to the large-area detection mechanism makes the detected light intensity spatially averaged and almost unaffected by interferometric noise fluctuations.

Major problems in the EDC approach are:

1. The efficiency of the FFE filter depends on the number of taps and on the relative spacing needed for impulse reconstruction. Due to the strong multipath dispersion usually encountered in legacy multimode fibers, several integral bit time equivalents are needed, leading to long FFE filter structures with more than 9 to 12 sections.
2. Increasing the number of taps leads to an increase in the equalization filter capability of the long pulse tail distortion, but at same time it increases considerably the power consumption and the design implementation complexity for the given technology state.
3. Internal delay of the EDC architecture must match with 10GbE bit-rate requirements (about 100 ps time step) and this leads to state-of-the-art CMOS (complementary metal oxide semiconductor) technology with less than a 90 nm gate length
4. The input stage must account for a linear automatic gain controlled (AGC) microwave amplifier with a proper dynamic range and a smooth bandwidth in excess of 8 GHz.
5. The optical photodetector and related low noise transimpedance amplifier must have a linear (V/W) transfer characteristic.
6. The DFE corrects only the pulse postcursor. Inherent leaking of the compensation capability of either pulse precursor and the dual peak pulse response reveal a severe limitation of the DFE approach for these pulse distortions.

1.6.2 Optical Mode Filtering (OMF)

The optical mode filtering (OMF) technique proposes a reduction in the number of propagating modes in the multimode fiber by selective excitation and detection of the fundamental fiber mode. Optical mode filtering can be summarized using the following basic operations:

1. A selective laser light launch into the multimode fiber input section in order to couple as much power as possible to the fundamental fiber mode only. This is achieved by means of a proper laser coupling mechanism in order to maximize the overlapping integral with the fundamental fiber mode.
2. Selective light detection at the multimode fiber end section by means of a spatial selective filter interposed between the multimode fiber end section and the photodetector active area.

By reducing drastically the number of excited mode groups, modal delay spreading is implicitly reduced. The principal problem encountered by this method is the large amount of power fluctuation (modal noise) induced by the standard connector offset and perturbing environmental conditions. However, under controlled laboratory conditions, this solution provided excellent results. From an application point of view, this solution requires specialized launch and detection tools that add complexity and cost to high-volume market demands. It is a common opinion of the IEEE 802.3aq

Committee that in order to introduce OMF as a valid signal compensation technique it should work together with EDC. Of course, the performance required in this case by EDC would be much less demanding than in a stand-alone application, but would still add more complexity and cost to the module final solution.

As had been anticipated, the basic principle behind OMF is to force as much multimode fiber as possible to operate as nearly single-mode fiber in the 1310 nm region by selective excitation and selective detection of the fundamental fiber mode. In the OMF approach, only the fundamental fiber mode would be excited in principle, leaving a relatively small contribution in terms of pulse energy carried up to the fiber end to the residually excited higher-order modes. In other words, the basic idea behind OMF is to force a single-mode regime into a multimode fiber. Although in principle the differential mode delay and the modal bandwidth concepts no longer apply to the OMF approach, the interferometric noise between excited higher-order modes and the fundamental mode grown at each fiber discontinuity, like connectors and fusion splices, makes the whole channel design much more critical with respect to optical alignment tolerances when compared to the EDC approach. Every misalignment in the fiber core contributes to unwanted higher-order mode excitation and modal noise. An additional effect is represented by the polarization of the fundamental mode respect to the direction connector misalignment. Due to the random nature of the polarization direction of the fundamental mode and to its sensitivity to any environmental condition, a polarization-dependent noise term must be added to light intensity. A careful central spot size launching condition, receiver mode filtering and optical connector alignment statistics all play a dominant role in the OMF approach. Unfortunately, standard tolerances for MMF technology optical connectors are too loose to compete with the OMF requirements. High modal noise due to an interference pattern between higher order modes and the fundamental mode severely limits system performance.

Major problems in the OMF approach are:

1. The laser source coupled field must match the fundamental fiber mode in order to transfer as much power as possible to that mode. This in particular requires numerical aperture adaptation between the laser light and the fundamental fiber mode.
2. Due to almost unavoidable irregularity of the refractive index profile at the fiber center (dip or pin) laser light should not be focused on such a small area around the fiber axis. Laser light should be applied to a larger axial-symmetric region in order to minimize the relative power coupled in the defective central region, but a region not too large to provide unwanted higher mode excitation.
3. Minimize the power transferred to higher-order modes.
4. Connector offset plays a dominant role in OMF penalty calculation. Any offset leads to power coupling that is not optimized, allowing higher-order mode excitation and consequent pulse dispersion.
5. Polarization and connector offset generate relevant modal noise.
6. The modal filter at the receiver end is needed to cut out higher-order mode contributions to the detected intensity, but it generates strong intensity fluctuations when modal noise, polarization and connector offset are produced simultaneously.

1.6.3 Quaternary Pulse Amplitude Modulation (PAM-4)

The basic idea behind the quaternary pulse amplitude modulation (PAM-4) proposal is to reduce the bandwidth requirement of the multimode fiber link in order to allow full 10GbE datastream transmission over a long-reach legacy multimode fiber link. This is achieved by using four-level modulation amplitude instead of the more conventional two-level NRZ (no return to zero) modulation scheme. Adopting the four-level scheme, each sequence of two information bits is coded

into the four-level digital amplitude instead of being simply time multiplexed, as shown by the following encoding logic:

b_1	b_2	L	$I_2 + I_1$	I_{mod}
0	0	L_0	$0+0$	0
0	1	L_1	$0+I$	I
1	0	L_2	$2I+0$	2I
1	1	L_3	$2I+I$	3I

This shows the encoding relations between the NRZ dual-bit sequence (b_1, b_2) and the logic PAM-4 levels L_k, $k = 0, 1, 2, 3$. Each PAM-4 logic level is then identified by combining the two current generators I_1 and I_2. The corresponding modulation current I_{mod}, reported in the last column, is injected into the laser.

The result is that for the same symbol rate exactly half a bit rate is required. Referring to the 10GbE signaling speed $B = 10.3125$ Gb/s, this translates into one-half of the symbol rate requirement, corresponding to exactly $B_{\text{PAM-4}} = \frac{1}{2}B = 5.156\,25$ Gb/s. Assuming that the multimode fiber modal bandwidth scales inversely with the link length (no mode group mixing), this leads to double the link length or one-half of the link bandwidth requirement for the fixed link length. Since there is interest in transmitting 10GbE, the latter conclusion looks quite attractive, allowing in principle 10GbE transmission over at least 300 m of legacy multimode fiber with a modal bandwidth $\widehat{BW}$ (bandwidth per kilometer) = 500 MHz km in the second window region.

Although the conclusion above could justify design efforts in the PAM-4 solution due to sensible relaxation of multimode fiber bandwidth requirements, major constraints will be added to the optoelectronic modules.

1.6.3.1 NRZ to PAM-4 Encoder

Figure 1.3 shows a solution for the PAM-4 encoder operating in the optical domain. The current encoding logic is represented by the following relationships:

$$\begin{cases} I_{\text{mod}} = I_1 + I_2 \\ I_{\text{L}} = I_{\text{mod}} + I_{\text{bias}} \end{cases}, \qquad \begin{cases} I_1 = \begin{pmatrix} I : \text{high} \\ 0 : \text{low} \end{pmatrix} \\ I_2 = \begin{pmatrix} 2I : \text{high} \\ 0 : \text{low} \end{pmatrix} \end{cases} \tag{1.5}$$

The laser diode driver LDD_1 delivers the modulation current I_1 that assumes two digital levels, namely $I_1 = I$ and $I_1 = 0$ in the high state and in the low state respectively. The laser diode driver LDD_2 delivers the modulation current I_2 that still assumes still two digital levels, but of double intensity, namely $I_2 = 2I$ and $I_2 = 0$ in the high state and in the low state respectively. According to the 1:2 demultiplexed function, each laser driver is fed at half the bit rate and each of them supplies the proper output current corresponding to the input digital level. Depending on the input dual-bit sequence, four input combinations are possible and correspondingly four output current levels are coded. Due to the 1:2 demultiplexed function, each output current level is associated with twice the input time step $T = 1/B$, effectively doubling the duration of each PAM-4 coded symbol.

The most relevant problem concerning the optical transmitter for the PAM-4 coding is the linearity of the laser characteristic and the resulting signal-to-noise ratio uniformity achievable for each level difference. It is well known that the laser pulse response is strongly dependent on the biasing position, at least when the laser is biased close to the lasing threshold. Different overshoot and transient time responses are therefore expected for the level transitions $L_0 \rightarrow L_1$ and $L_2 \rightarrow L_3$, due to the different positions of L_0 and L_2 respectively compared to the lasing threshold.

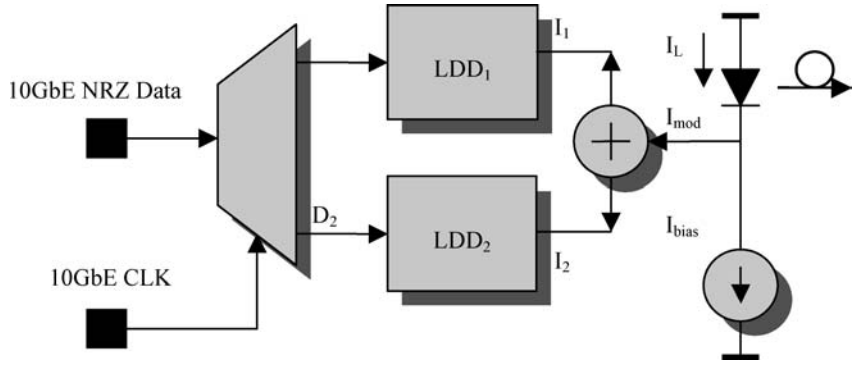

Figure 1.3 Block diagram of the NRZ to PAM-4 optical encoder. The modulation current is given by the sum of the two current components I_1 and I_2

In order to understand the signal differences better, Figure 1.4 illustrates both the NRZ signal and the corresponding PAM-4 converted signal. The first row in Figure 1.4 shows the incoming NRZ pattern. The following two waveforms represent the 1:2 demultiplexed signals with ideal timing. In order to align those waveforms it is necessary to add a time delay equal to one time step T to waveform D_1. The resulting shifted signal is then represented. The current sum shown in the schematic in Figure 1.3 therefore provides the PAM-4 output reported. This is the modulation current pattern that drives the semiconductor laser.

1.6.3.2 PAM-4 to NRZ Decoder

Once the optical PAM-4 signal reaches the photodetector it must be recognized and converted to NRZ using a proper PAM-4 to NRZ decoder. Figure 1.5 gives the block diagram for a plausible solution for the PAM-4 to NRZ decoder.

The basic principle underlying the schematic PAM-4 to NRZ decoder presented in Figure 1.5 considers the three inner level transitions of the PAM-4 signal to be three separate NRZ signals of reduced amplitude. After detection, the logic block recovers the original NRZ pattern. The major constraint in the PAM-4 to NRZ decoder is the reduced signal-to-noise ratio available at each threshold detector in the optical receiving process in comparison to the equivalent NRZ optical receiver. It is important to underline the fact that the comparison between NRZ and PAM-4 optical receivers should be performed using adequate assumptions and available technology.

1.6.3.3 NRZ versus PAM-4: SNR Comparison

In order to calculate the signal-to-noise ratio and proceed to evaluate the different benefits and impairments between NRZ and PAM-4 modulation schemes, consider the following assumptions:

1. NRZ and PAM-4 optical receivers use the same IC technology with the same white thermal noise power spectral density n_{th}. This allows only noise bandwidth differences to be considered as responsible for the different noise powers available in the two receivers.
2. Both optical receivers are thermal noise limited. In other words, thermal noise is the dominant contribution in setting the sensitivity performances.
3. NRZ and PAM-4 optical receivers both have the same frequency response profile, but the NRZ receiver has twice the bandwidth of the PAM-4 receiver.

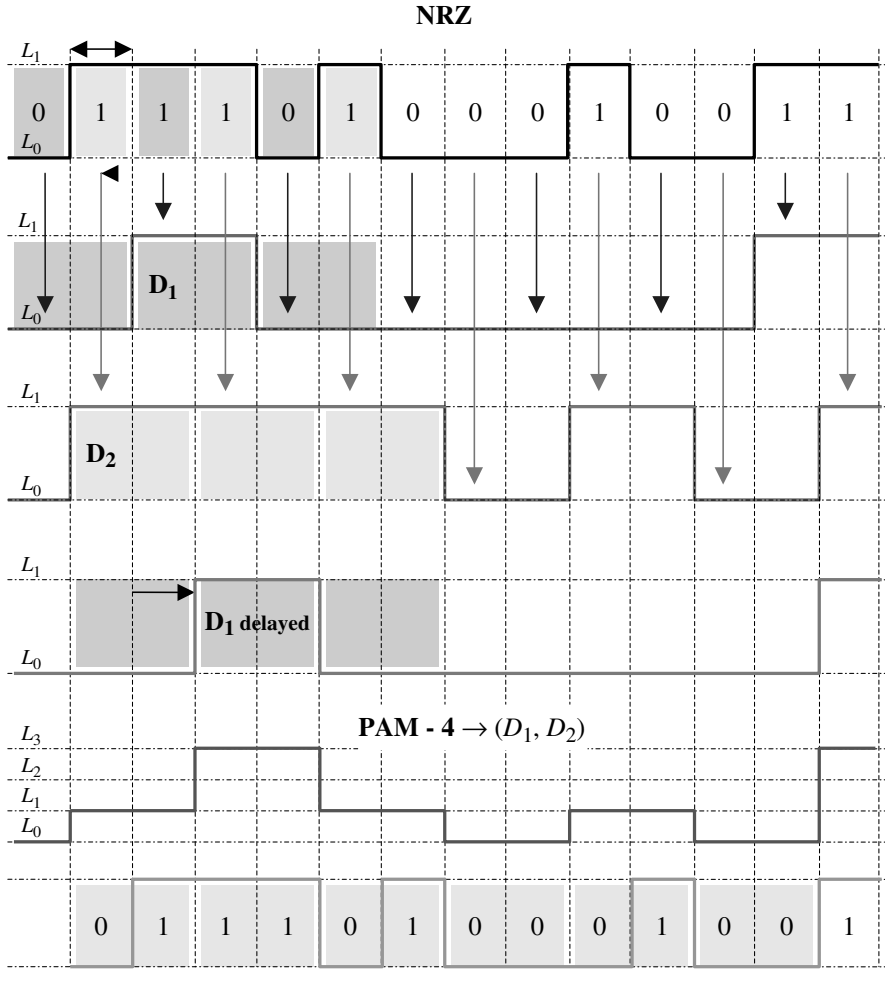

Figure 1.4 NRZ to PAM-4 signal encoding according to the block diagram presented in Figure 1.3. Light waveforms are detected at the 1:2 demultiplexed output including T-delay required in order to align signal wavefronts before the current sum. The waveform shows the total modulation current injected into the laser according to the coded PAM-4 pattern

Figure 1.6 is a schematic representation of the frequency response and related noise bandwidth of both receivers. According to the third assumption, the two receivers have a noise bandwidth ratio equal to their corresponding bandwidths. Therefore:

$$B_{\mathrm{n,NRZ}} = 2B_{\mathrm{n,PAM\text{-}4}} \tag{1.6}$$

From assumptions 1 and 2, it can easily be deduced that the noise power of the NRZ receiver is twice the noise power of the PAM-4 receiver:

$$\sigma^2_{\mathrm{n,NRZ}} = B_{\mathrm{n,NRZ}} n_{\mathrm{th}} = 2B_{\mathrm{n,PAM\text{-}4}} n_{\mathrm{th}} = 2\sigma^2_{\mathrm{n,PAM\text{-}4}} \tag{1.7}$$

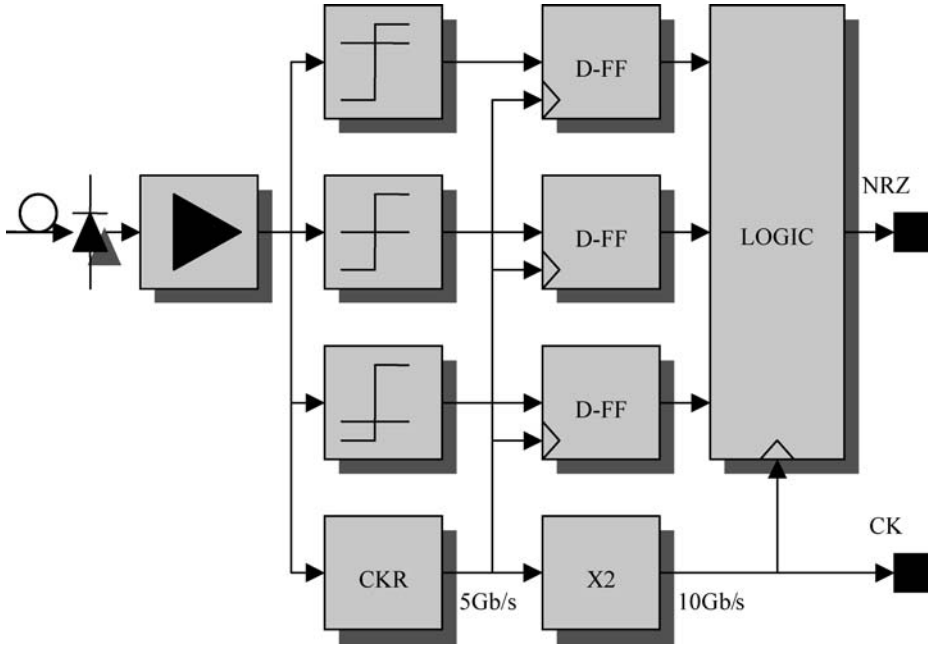

Figure 1.5 Schematic representation of the block diagram of a PAM-4 to NRZ decoder using three threshold detectors and a clock by 2 multiplier. By choosing the correct threshold position of the three threshold detectors, the subsequent logic can reconstruct the original NRZ signal from the PAM-4 detected signal

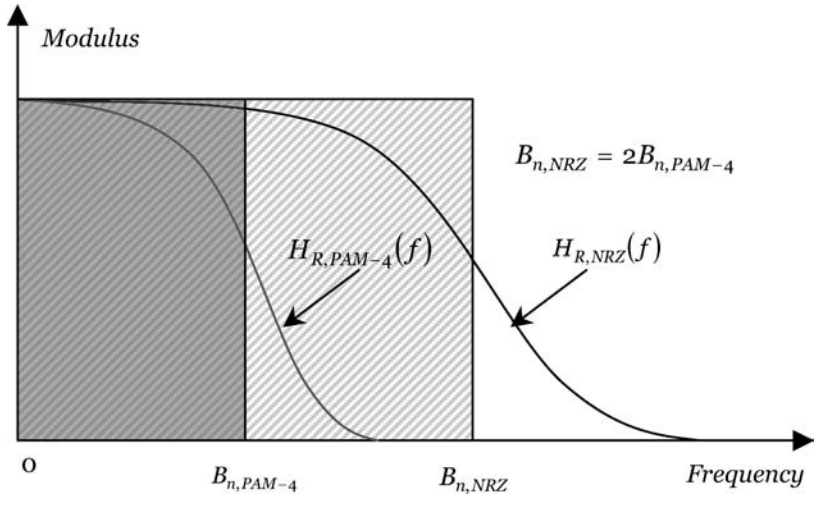

Figure 1.6 Schematic representation of frequency responses and noise bandwidths of NRZ and PAM-4 receivers. According to the third assumption, noise bandwidths have the same ratio of $\frac{1}{2}$ as their respective cut-off frequencies

The RMS (root mean square) noise reduction Δ_n produced using the PAM-4 receiver can be estimated as

$$\Delta_n \equiv 10\log_{10}\left(\frac{\sigma_{n,NRZ}}{\sigma_{n,PAM\text{-}4}}\right) = 10\log_{10}\sqrt{2} \cong 1.5 \text{ dB(optical)} \tag{1.8}$$

The gain factor Δ_n represents the average optical power sensitivity improvement for achieving the same signal-to-noise ratio performances for a given signal amplitude. If the required decision threshold distance had been the same for both NRZ and PAM-4 receivers, it can be concluded that there is a net gain of 1.5 dB (optical) when using the PAM-4 solution versus the NRZ one, but unfortunately this is not the case. In fact, for a given average received optical power P_R, the PAM-4 signal has a one-third decision amplitude with respect to the corresponding NRZ signal. The signal pattern reported in Figure 1.4 gives a qualitative representation of this characteristic behavior. Figure 1.7 shows the computed gain between the PAM-4 and the NRZ line coding versus increasing multimode fiber link length for a specified modal bandwidth of $\widehat{BW} = 500$ MHz km with Gaussian frequency response. Figures 1.8 and 1.9 show instead a more realistic computer simulation of both NRZ and PAM-4 eye diagrams, assuming that they have the same average optical power for the 10GbE case. The pulse has been chosen according to the raised cosine family with unit roll-off.

Since there is no intersymbol interference (ISI) in both cases, the reduction in the decision amplitude experienced for each signal transition in the PAM-4 pattern with respect to the NRZ one

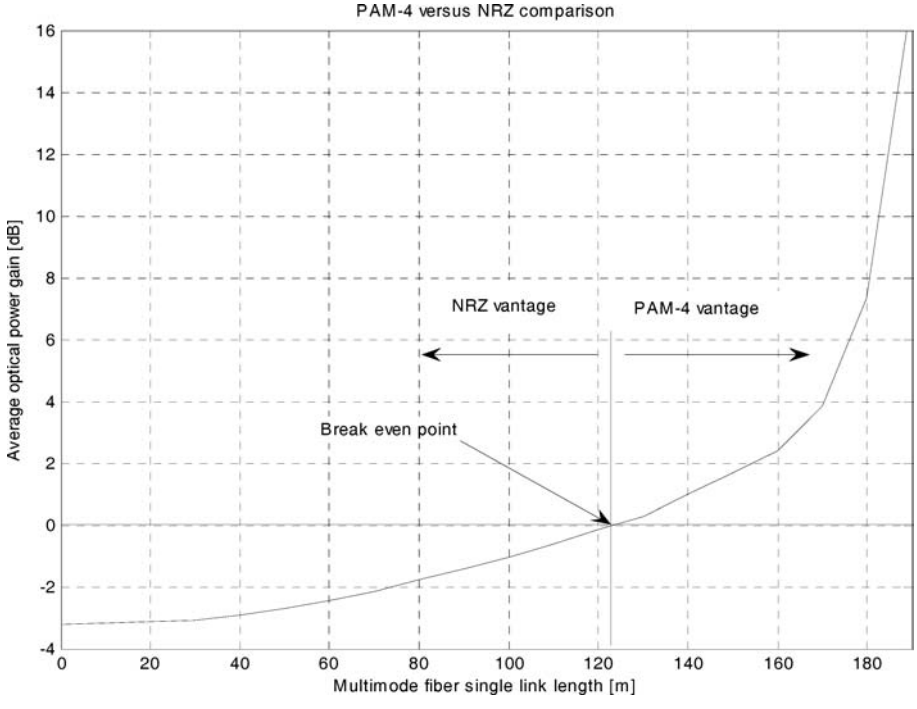

Figure 1.7 Optical sensitivity gain comparison between the PAM-4 and NRZ line codings versus the multimode fiber single link length. The fiber modal bandwidth is $\widehat{BW} = 500$ MHz km. The breakeven distance is about $L_0 = 123$ m

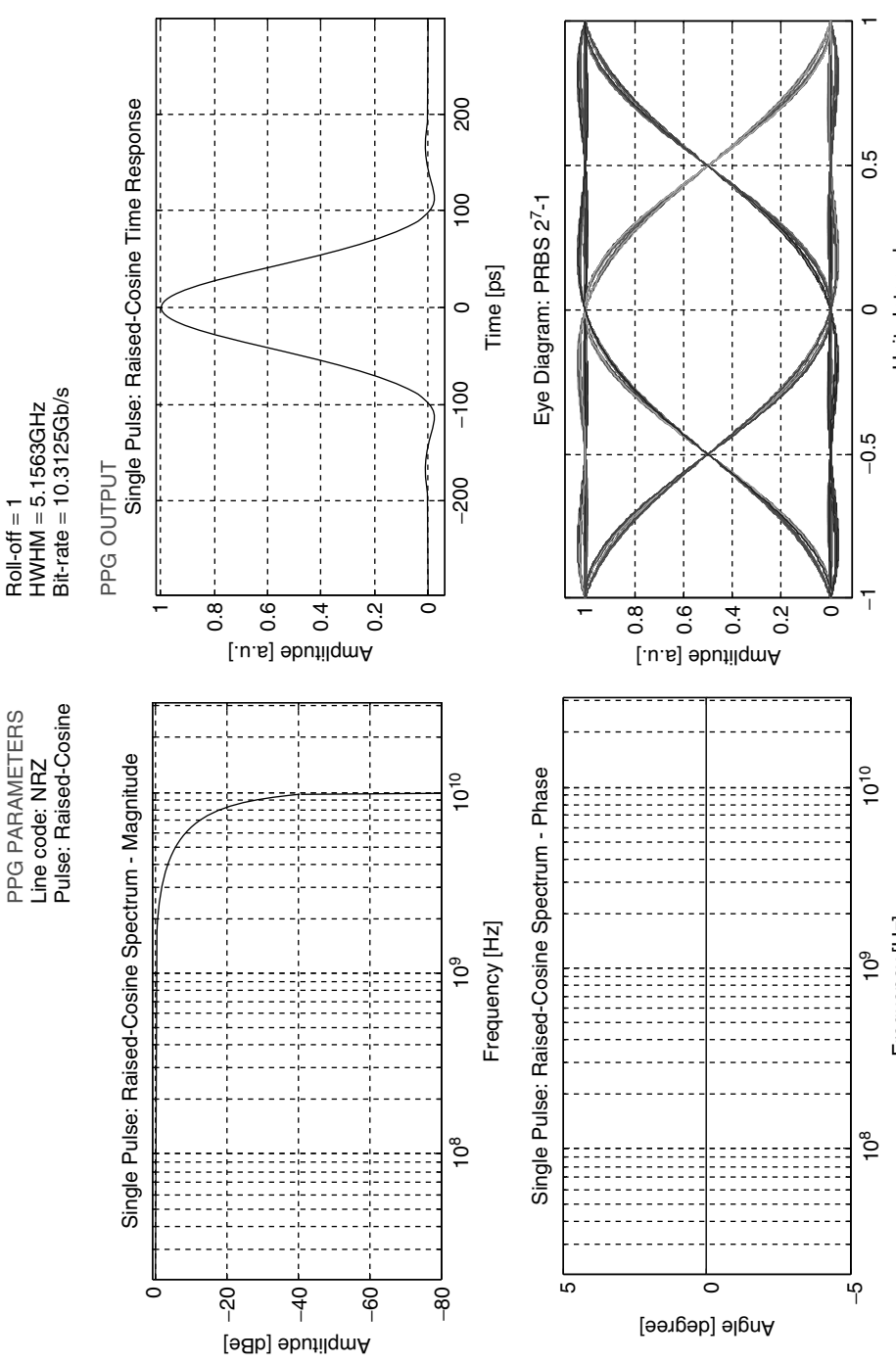

Figure 1.8 Frequency and time domain representations of NRZ PRBS 2^7-1 line code signals at 10GbE data rate. Left top represents the single pulse according to the unity roll-off raised cosine profile, while the left bottom graph shows the corresponding eye diagram in normalized bit time units

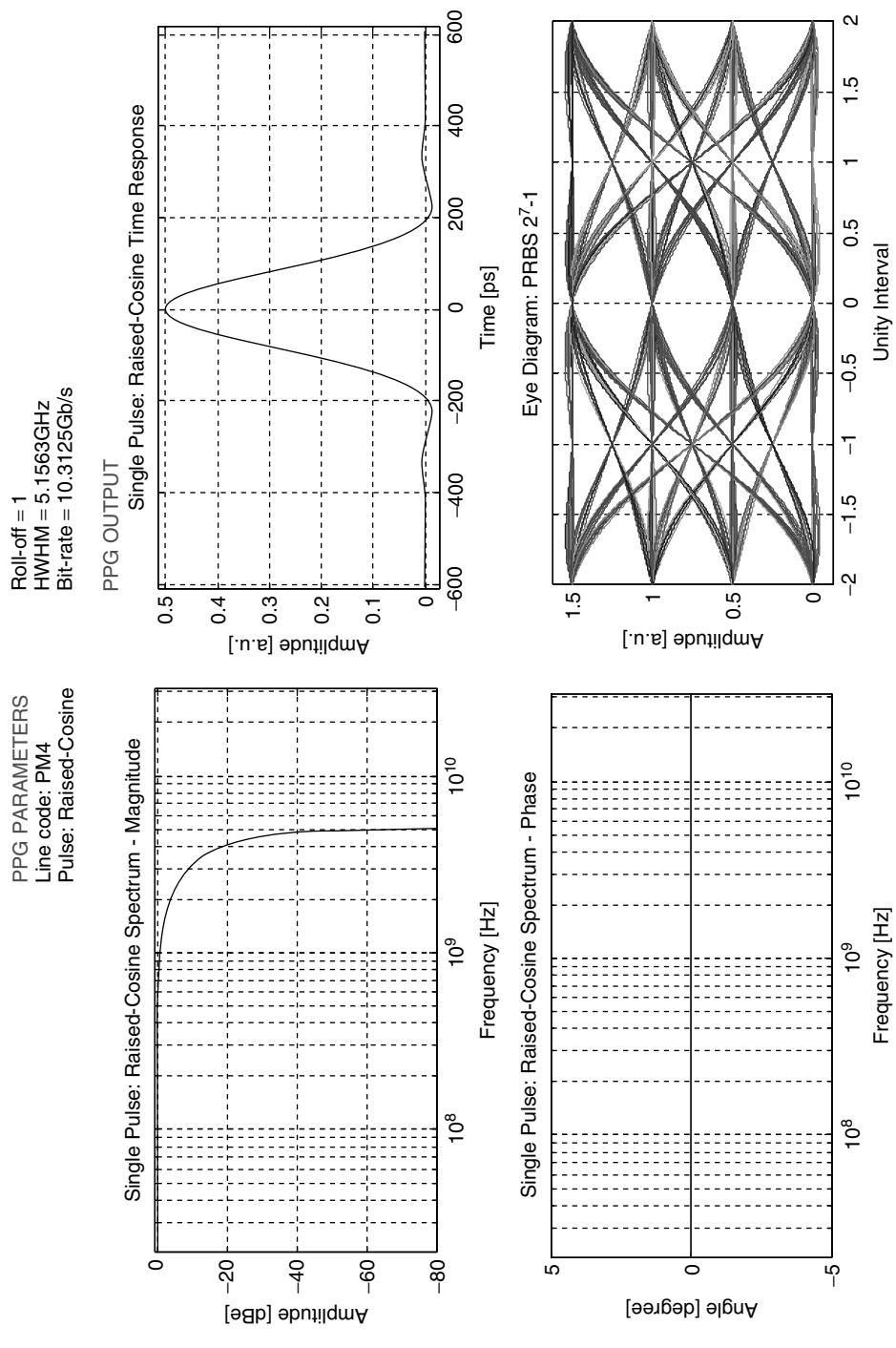

Figure 1.9 Frequency and time domain representations of PAM-4 PRBS 2^7-1 line code signals at 10GbE data rate. Left top represents the single pulse according to the unity roll-off raised cosine profile, while the left bottom graph shows the corresponding eye diagram in normalized bit time units. A scaling factor of 2 has been introduced in the raised cosine pulse profile with respect to the NRZ case shown above

leads to a loss of signal strength of about 4.77 dB (optical):

$$\Delta_s = 10\log_{10}(1/3) \cong -4.77\,\text{dB} \tag{1.9}$$

This value refers to ideal eye diagrams with no added jitter or ISI and the average eye opening coincides with the decision threshold amplitude for each level. The receiver sensitivity for a given bit error rate (BER) is determined by the Q-factor defined below, where d is the decision threshold distance and σ is the total RMS noise amplitude. Assuming thermal noise limited detection and Gaussian noise approximation, then

$$Q \equiv \frac{d}{\sigma}, \qquad \text{BER} = \frac{1}{2}\text{erfc}\left(\frac{Q}{\sqrt{2}}\right) \tag{1.10}$$

Taking into account the reduced noise bandwidth in Equation (1.8) for PAM-4 and the corresponding detection amplitude reduction in Equation (1.9), it can be concluded that the net average optical power gain using the PAM-4 receiver instead of the corresponding NRZ receiver is about 3.27 dB (optical):

$$\Delta_Q = \Delta_s + \Delta_n \cong -4.77 + 1.50 = -3.27\,\text{dB} \tag{1.11}$$

This is essentially the reason for the success of the NRZ solution adopted in almost all optical telecommunication systems. Of course, at least technically the development of the PAM-4 signaling must be justified.

1.6.3.4 NRZ versus PAM-4: Eye Opening Comparison

The general signal-to-noise reduction experienced by the PAM-4 signal must in fact be balanced by the reduced channel bandwidth requirement, as clearly shown by comparing the left top graphs of Figures 1.8 and 1.9. Assuming the same unity roll-off raised cosine signal pulse profile in both modulation codes, it is evident that the PAM-4 pulse requires exactly a bandwidth that is one-half of the corresponding NRZ case. This leads to a considerable pulse spreading reduction after a given link length propagation, which corresponds to a relative increased optical eye opening. Following this reasoning, it is possible to arrive at the obvious conclusion justifying the PAM-4 coding when reduced transmission channel capabilities must be accounted for in the transmission system design.

Figures 1.10 and 1.11 report respectively the PAM-4 and NRZ data stream detected after a single link length of 100 m of a Gaussian bandwidth multimode fiber. Most of the original eye opening reduction due to multilevel coding has been recovered after just 100 m of link length. In fact, the PAM-4 eye opening diagram results from about 27 % of the highest PAM-4 signal amplitude, while the same qualitative calculation performed on the NRZ eye diagram shows that the eye opening results from about 50 %. Referring to the ideal −4.77 dB penalty reported in Equation (1.9), the ratio now gives about −2.67 dB, with a recovery of about 2.1 dB. Assuming the same noise spectral power density for both line codes, the net gain in using PAM-4 versus NRZ is still negative, −1.17 dB, but is much more reduced compared to the back-to-back case in Equation (1.11).

The relative performance of PAM-4 line coding improves at longer link lengths, as shown in Figures 1.12 and 1.13 for the case of a single link length of 150 m of the same Gaussian bandwidth multimode fiber. A qualitative eye opening measurement for both cases gives about the same value of 18 %, leading to a positive net gain of 1.5 dB, which coincides with the noise bandwidth enhancement factor. The breakeven point in using PAM-4 instead of NRZ for this Gaussian bandwidth multimode fiber is therefore somewhere between 100 m and 150 m, where the net gain is zero. For every longer link length, PAM-4 gives theoretically better performances than NRZ.

The last simulated case shown in Figures 1.14 and 1.15 refers to a single link length of 200 m of the same Gaussian bandwidth multimode fiber. The PAM-4 eye diagram looks almost closed, even

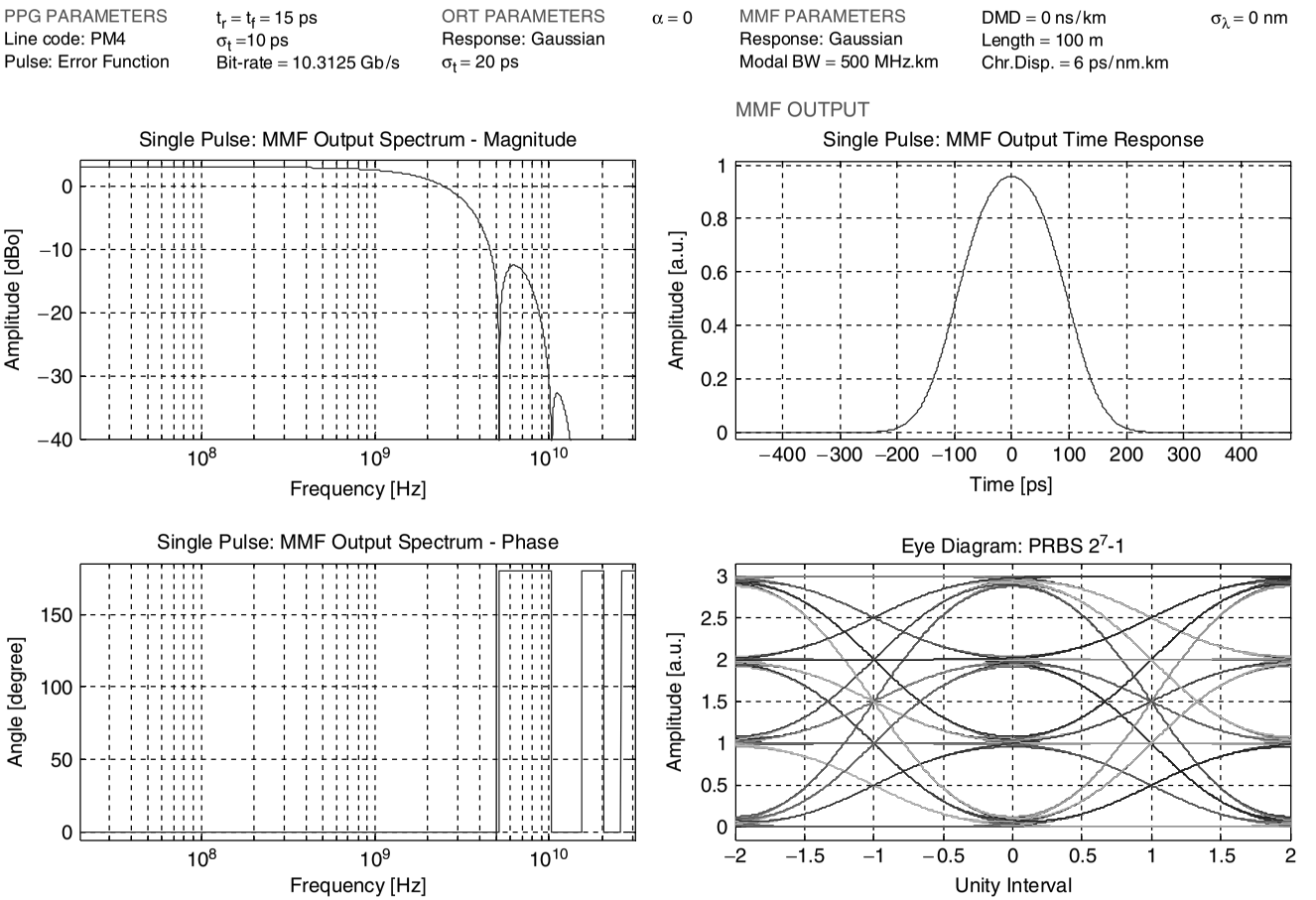

Figure 1.10 Frequency and time domain representations of PAM-4 PRBS 2^7-1 line code signals at 10GbE data rate after a 100 m single link length of Gaussian bandwidth multimode fiber. Left top represents the single pulse fiber output, while the left bottom graph shows the corresponding eye diagram in normalized bit time units. The legend at the top reports the simulated conditions for the pulse pattern generator and the light source impulse response

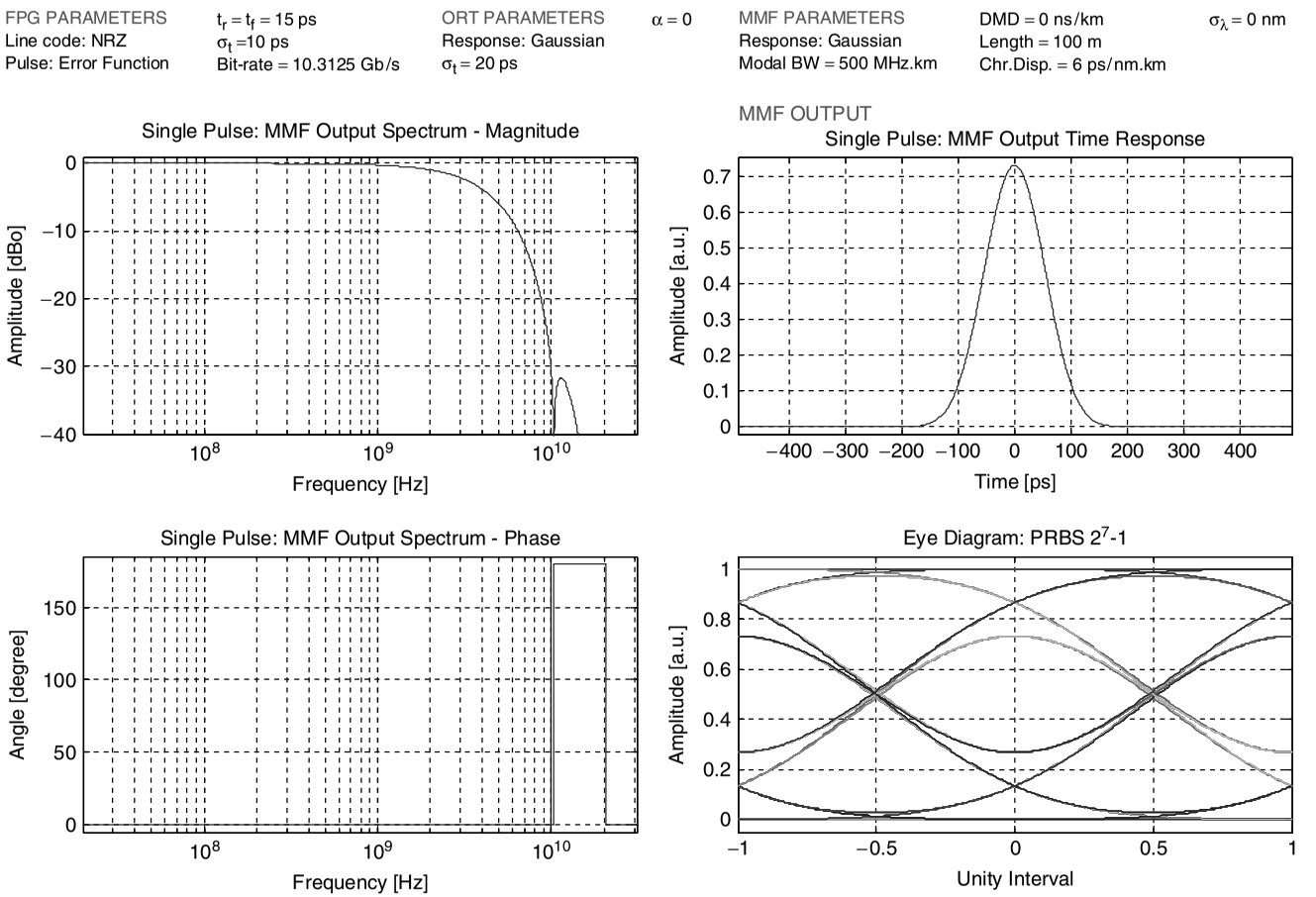

Figure 1.11 Frequency and time domain representations of NRZ PRBS 2^7-1 line code signals at 10GbE data rate after a 100 m single link length of Gaussian bandwidth multimode fiber. Left top represents the single pulse fiber output, while the left bottom graph shows the corresponding eye diagram in normalized bit time units. The legend at the top reports the simulated conditions for the pulse pattern generator and the light source impulse response

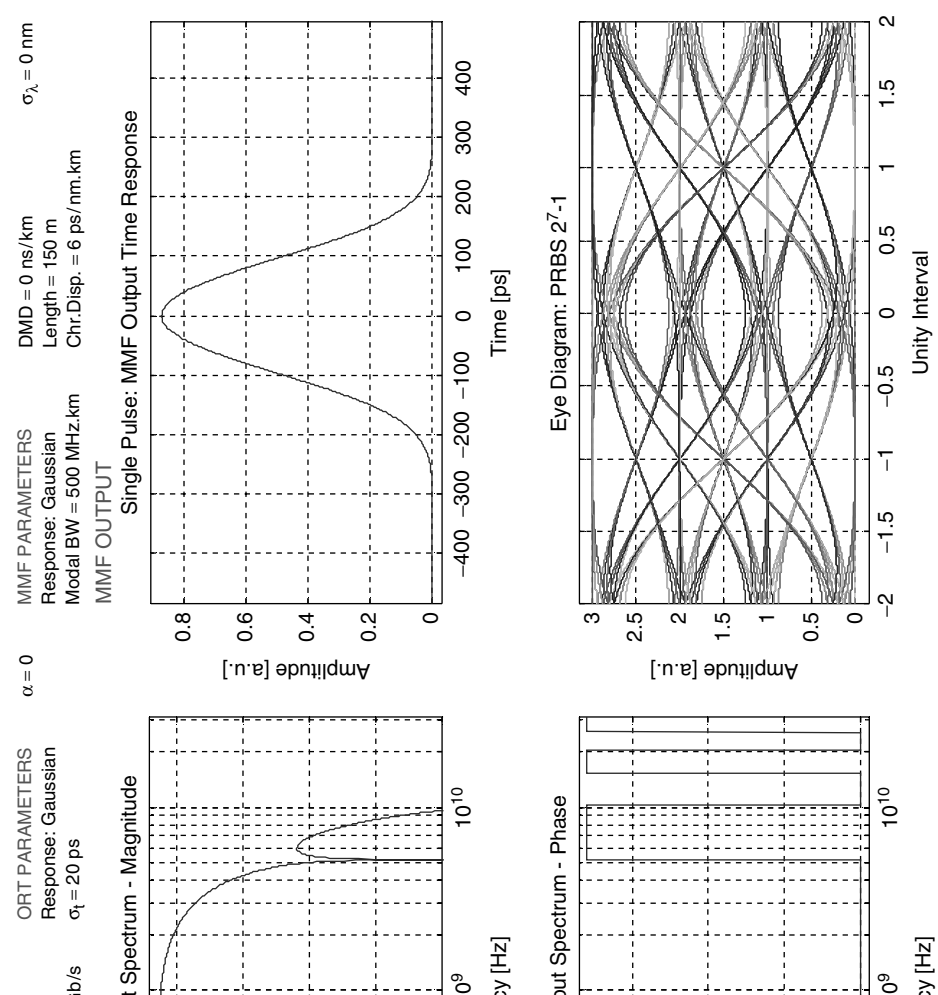

Figure 1.12 Frequency and time domain representations of PAM-4 PRBS 2^7-1 line code signals at 10GbE data rate after a 150 m single link length of Gaussian bandwidth multimode fiber. Left top represents the single pulse fiber output, while the left bottom graph shows the corresponding eye diagram in normalized bit time units. The legend at the top reports the simulated conditions for the pulse pattern generator and the light source impulse response

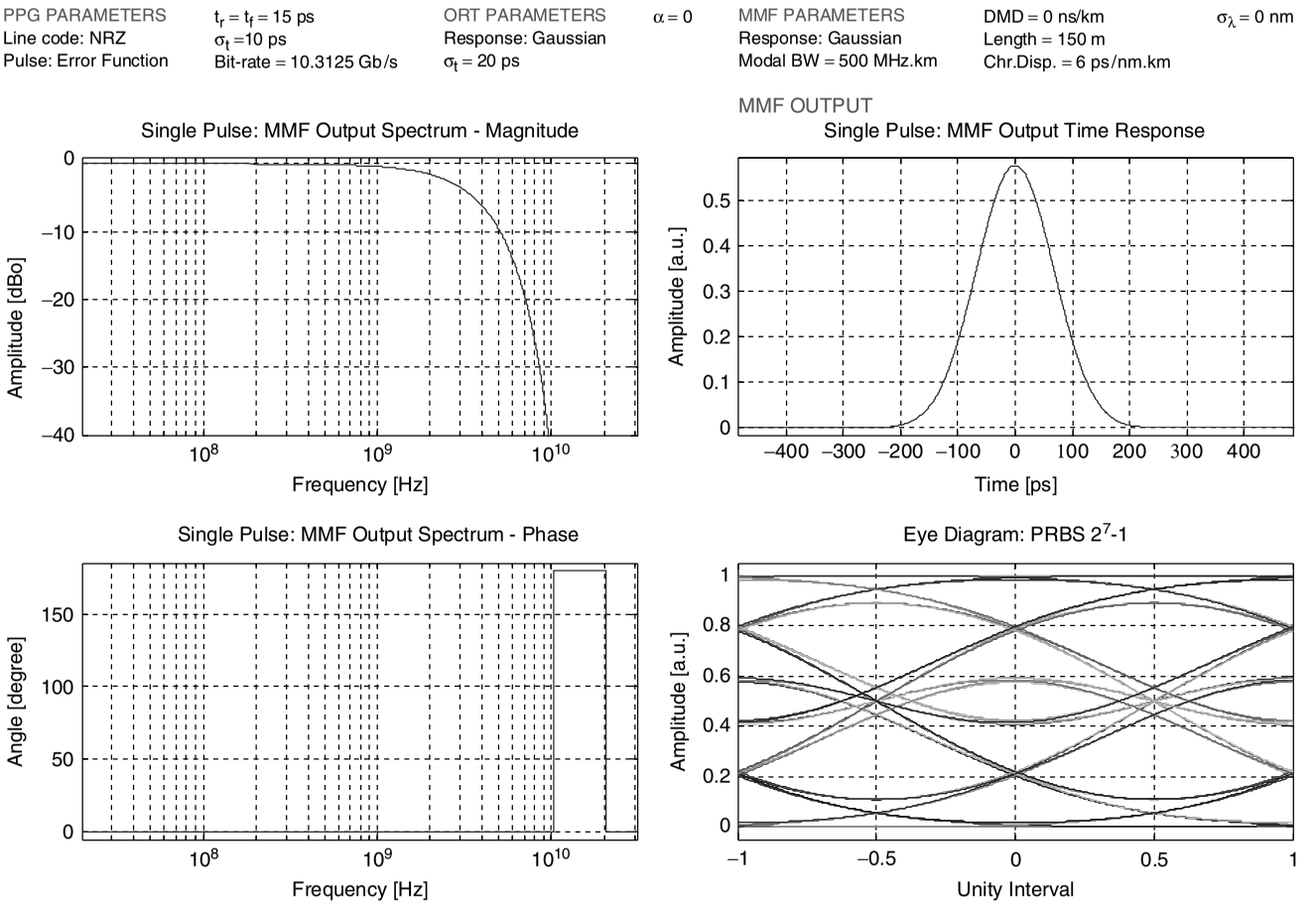

Figure 1.13 Frequency and time domain representations of NRZ PRBS 2^7-1 line code signals at 10GbE data rate after a 150 m single link length of Gaussian bandwidth multimode fiber. Left top represents the single pulse fiber output, while the left bottom graph shows the corresponding eye diagram in normalized bit time units. The legend at the top reports the simulated conditions for the pulse pattern generator and the light source impulse response

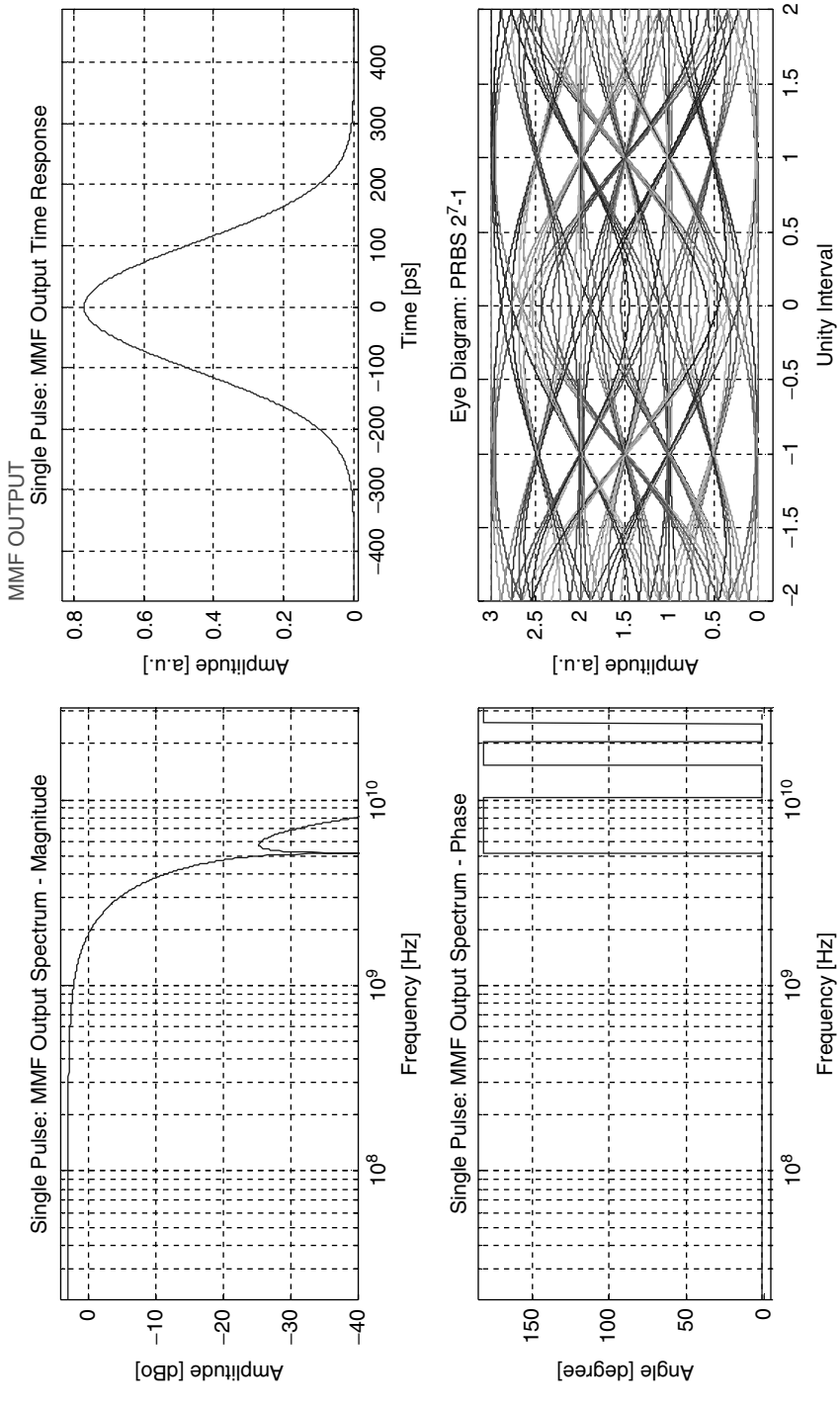

Figure 1.14 Frequency and time domain representations of PAM-4 PRBS 2^7-1 line code signals at 10GbE data rate after a 200 m single link length of Gaussian bandwidth multimode fiber. Left top represents the single pulse fiber output, while the left bottom graph shows the corresponding eye diagram in normalized bit time units. The legend at the top reports the simulated conditions for the pulse pattern generator and the light source impulse response